Science of Remote Sensing 10 (2024) 100164

Contents lists available at ScienceDirect

Science of Remote Sensing

journal homepage: www.sciencedirect.com/journal/science-of-remote-sensing

Use of light response curve parameters to estimate gross primary production capacity from chlorophyll indices of global observation satellite and flux data

Kanako Muramatsu [a,b,*], Emi Yoneda [b], Noriko Soyama [c], Ana López-Ballesteros [d], Juthasinee Thanyapraneedkul [e]

[a] Department of Chemistry, Biology, and Environmental Science, Faculty of Science, Nara Women's University, Kitauoyanishi-machi, Nara, 630-8506, Japan
[b] Department of Information and Computer Sciences, Graduate School of Science, Nara Women's University, Kitauoyanishi-machi, Nara, 630-8506, Japan
[c] Faculty of Human Studies, Tenri University, 1050, Somanouchi, Tenri, Nara, 632-8510, Japan
[d] Department of Agricultural and Forest Systems and the Environment, Agrifood Research and Technology Centre of Aragon (CITA), Avda. Montañana 930, 50059, Zaragoza, Spain
[e] Department of Environmental Science, Faculty of Science and Technology, Thammasat University, Pathumthani Province, 12120, Thailand

ARTICLE INFO

Keywords:
CI_{green}
Eddy covariance flux
GPP
Light response curve
MODIS
Rectangular hyperbola equation

ABSTRACT

The photosynthetic rate has a nonlinear relationship with PAR during the day. We previously developed an algorithm for estimating GPP capacity, which is defined GPP under low-stress condition, using light response curves (LRCs). In this study, we studied the characteristics of LRC parameters of the initial slope and the maximum gross photosynthesis rate (P_{max}), and formulas to calculate P_{max} from the relationship between the chlorophyll index of the green and near-infrared (NIR) bands (CI_{green}) and the GPP capacity at PAR = 2000 μmol m^{-2} s^{-1} (GP2000) for nine vegetation types spanning tropical to subarctic climates on the Eurasian and North American continents using eddy covariance flux measurements and Moderate Resolution Imaging Spectrometer (MODIS) data. The slope of the relationship between CI_{green} and GP2000 was highest for sites dominated by herbaceous plants such as open shrubland, savanna, and cropland (rice paddy); it was lower at sites dominated by woody plants. The yearly GPP/GPP capacity ratio was close to one in flux data. When the method was applied to satellite data, the daily GPP capacity exhibited a similar seasonal pattern to that of the Flux GPP and MODIS GPP products. Under high dryness conditions, Flux GPP showed the drop from the GPP capacity estimated from CI_{green} and diurnal PAR data around noon, and they were nearly identical during the early morning and late afternoon. The instantaneous GPP capacity could be considered the baseline of the instantaneous GPP with stress-free conditions and important for quantifying midday depression at the sub-day scale.

1. Introduction

Accurate observations of CO_2 exchange between the canopies of different types of plants and the atmosphere are crucial for understanding the carbon cycle and land–atmosphere feedback processes in climate change scenarios. Gross primary production (GPP), which represents the total amount of CO_2 absorbed by plants through photosynthesis, accounts for the largest global carbon flux (Beer et al., 2010). Satellite remote sensing (e.g., the Earth Observing System) can monitor vegetation phenology globally and has been used to estimate GPP using models based on light use efficiency (LUE) (Monteith, 1972; Heinsch et al., 2006). Such models assume a linear relationship between GPP and photosynthetically active radiation (PAR), with the incorporation of LUE (ϵ) as a coefficient as follows:

$$GPP = \epsilon f_{APAR\_canopy} PAR \quad (1)$$

where f_{APAR_canopy} is the fraction of PAR absorbed by the plant canopy, which is estimated from the normalized vegetation index (NDVI) (Myneni and Williiams, 1994; Rouse et al., 1973) or from the inversion of the three-dimensional radiation transfer of surface reflectance in vegetation canopies (Myneni et al., 2002). This parameter is

* Corresponding author. Department of Chemistry, Biology, and Environmental Science, Faculty of Science, Nara Women's University, Kitauoyanishi-machi, Nara, 630-8506, Japan.
E-mail address: muramatu@es.nara-wu.ac.jp (K. Muramatsu).

https://doi.org/10.1016/j.srs.2024.100164
Received 8 November 2022; Received in revised form 5 September 2024; Accepted 9 September 2024
Available online 13 September 2024

significantly affected by non-photosynthetic canopy components such as stems and litter (Asner et al., 1998). When estimating GPP, photosynthetically active vegetation (mostly green leaves) should be distinguished from non-photosynthetically active vegetation (Xiao et al., 2004a, 2004b). Xiao et al. developed a vegetation photosynthesis model (VPM) using the fraction of APAR attributable to photosynthetically active vegetation (f_{APAR_PAV}) in plant canopies. The parameter is estimated using the enhanced vegetation index (EVI) (Huete et al., 1997) because the seasonal dynamics of EVI agree well with the observed GPP of temperate deciduous broadleaf forests and boreal–northern evergreen needleleaf forests during the growing season (Xiao et al., 2004aa;b).

GPP estimation models that focus on chlorophyll have been proposed based on a concept similar to the LUE-based model. For boreal forests, chlorophyll-absorbed PAR ($APAR_{chl}$) is strongly related to gross ecosystem production flux, whereas canopy-absorbed PAR ($APAR_{canopy}$) is only weakly related, as revealed by Moderate Resolution Imaging Spectrometer (MODIS) observations (Zhang et al., 2009). For deciduous broadleaf forests, the Medium Resolution Image Spectrometer (MERIS) terrestrial chlorophyll index (MTCI) (Dash and Curran, 2004; 2007, 2010) is strongly correlated with daily GPP based on flux observations. The EVI from MODIS is also strongly correlated with GPP. Differences between the MTCI and EVI indices are apparent in time series in which there is a greater time lag between the onset of the depression in GPP at the end of season and a downturn in the EVI (Harris and Dash, 2010). For crops (Gitelson et al., 2006; Peng and Gitelson, 2012) and mixed temperate forests (Croft et al., 2015), midday GPP has a strong linear relationship with the total chlorophyll content in the canopy multiplied by the PAR.

The photosynthetic rate is not linearly related to PAR at the leaf scale and often not at the canopy scale. To include this nonlinearity in GPP estimation models, light-response curves (LRCs) of the GPP and PAR relationship have been used (Furumi et al., 2005; Harazono et al., 2009; Ide et al., 2010). The maximum gross photosynthesis rate (P_{max}) in the GPP–PAR curve is determined from the relationship between the vegetation index and observed GPP. During the midday period, the photosynthetic rate often decreases due to stomatal closure in dry weather conditions (Pathre et al., 1998; Pessarakli, 2005), and this is not related to chlorophyll content in leaves. These levels are related to the light reactions involved in photosynthesis, and stomatal opening and closure is related to the carbon reduction cycle. Thus, the estimation of GPP can be separated according to these two phenomena (Thanyapraneedkul et al., 2012). Here, we focus on the former, and defined the GPP capacity as GPP under low-stress conditions. To estimate this capacity, we use a GPP capacity–PAR, which estimates the relationship in the form of a rectangular hyperbola. It is assumed that the P_{max} at light saturation under low-stress conditions is mainly dependent on the total chlorophyll content in a canopy. We replace this with the GPP capacity at a PAR that is sufficiently high at 2000 μmol m^{-2} s^{-1} (hereafter, GP2000). This has a linear relationship with the chlorophyll index (CI) of the green and near-infrared band (CI_{green}), which is strongly correlated with chlorophyll content (Gitelson et al., 2006; Thanyapraneedkul et al., 2012). It is a close proxy of plant absorption coefficients in the green spectral region (Gitelson et al., 2019).

The advantage of a model using the GPP capacity–PAR curve is that the diurnal variation in the GPP capacity can be calculated, as shown in Fig. 1. This GPP capacity is considered the baseline, which is the GPP under unstressed conditions. The midday depression is the area between the baseline and the GPP (Muramatsu, 2018). We have previously examined the parameters of the GPP capacity curve in North America, Japan, and Thailand, for the following types of vegetation cover recognized by the International Geosphere Biosphere Program (IGBP): open shrubland, savanna, grassland, cropland (rice paddy), closed shrubland (permanent wetland), deciduous needleleaf forest, evergreen needleleaf forest, and evergreen broadleaf forest (Thanyapraneedkul

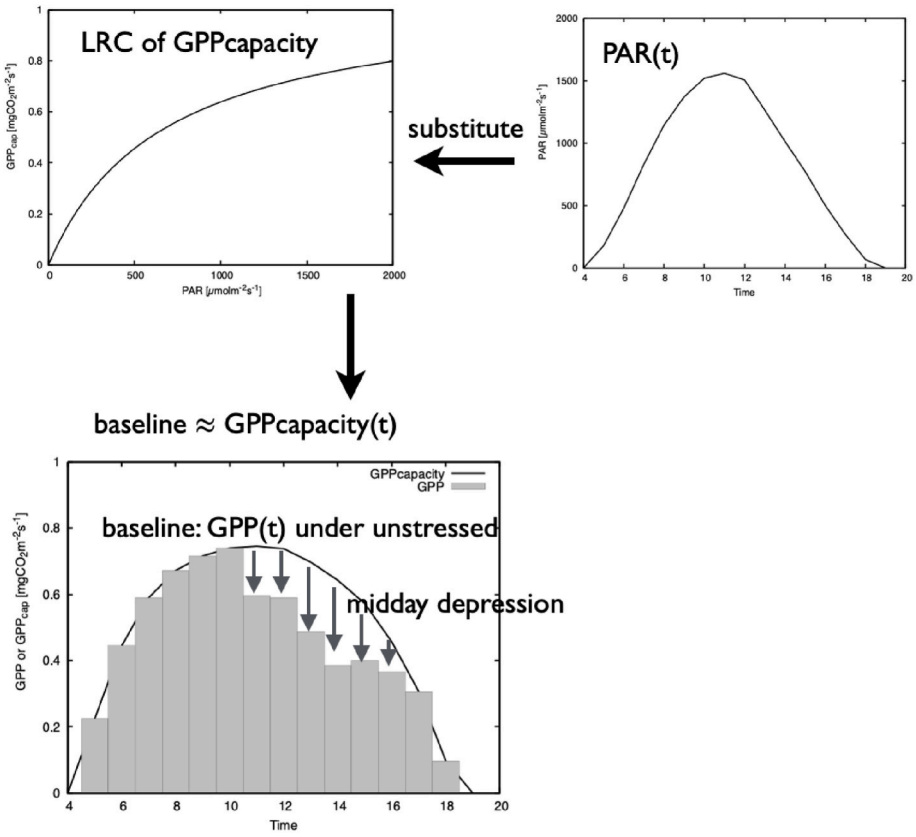

Fig. 1. Diurnal variation in instantaneous GPP capacity can be calculated from light response curve of GPP capacity and diurnal variation in photosynthetically active radiation (PAR). Baseline is defined as GPP under unstressed conditions, and GPP capacity is considered the baseline for midday depression.

et al., 2012; Mineshita et al., 2016; Muramatsu et al., 2017). Plants in Europe, including Siberia, belonging to subarctic climate regions, have not yet been analyzed and should be evaluated to ascertain whether the rules governing the parameters of plant functional types differ among continents with subarctic to tropical climates. It is unclear whether the parameters and relationship between GP2000 and CI_{green} vary among vegetation types. Thus, in this study, we examined these characteristics among different vegetation types and examined the daily and diurnal variation in GPP capacity estimated from MODIS CI_{green} in comparison with MODIS GPP and Flux GPP.

2. Data and methods

2.1. Background: LRC formula

We used an LRC for canopy GPP capacity (Thanyapraneedkul et al., 2012), as follows:

$$GPP_{capacity}(PAR(t)) = \frac{\alpha P_{max} PAR(t)}{1 + \alpha PAR(t)} \quad (2)$$

where α (m^2 s (μmol photon)$^{-1}$) is a parameter related to the initial slope, P_{max} ($mgCO_2$ m^{-2} s^{-1}) is considered the maximum rate of canopy gross photosynthesis at light saturation, αP_{max} is the initial slope of the LRC and represents the apparent quantum efficiency under weak light conditions. GP2000, already described above (Fig. 2), can be estimated (Thanyapraneedkul et al., 2012; Mineshita et al., 2016; Muramatsu et al., 2017) using the green CI (CI_{green}) (Gitelson et al., 2006) based on satellite reflectance data in the near infrared (R_{NIR}) and green (R_{green}) bands as follows:

$$GP2000 = aCI_{green} + b \quad (3)$$

$$CI_{green} = \frac{R_{NIR}}{R_{green}} - 1 \quad (4)$$

Another rectangular hyperbola LRC formula is often used:

$$GPP(PAR(t)) = \frac{QP_{max} PAR(t)}{P_{max} + QPAR(t)} \quad (5)$$

where Q is the apparent quantum efficiency and is the initial slope of the LRC; P_{max} is the maximum rate of GPP. Equations (2) and (5) are the same when the relationship between the parameters in both formulas is $\alpha = Q/P_{max}$. We used a rectangular hyperbola equation to reduce the number of parameters. Owen et al. (2007) showed that when the theoretical maximum CO_2 uptake capacity at a high light intensity of 2000 (μmol m^{-2} s^{-1}) is expressed as a rectangular hyperbola, the value is similar to that obtained from a non-rectangular hyperbola equation.

2.2. Data collection sites for different IGBP classes and fluxes

Flux data were obtained for nine IGBP vegetation classes (Steffen et al., 1992). Table 1 lists the collection sites. Flux data from Europe (http://www.europe-fluxdata.eu/home) and Siberia Asia (http://www.asiaflux.net) were used to determine the LRC parameters. For the European sites (ES-Agu, FR-Hes, NL-Loo, IT-Lav, and FR-Pue), GPP and vapor pressure deficit (VPD) data were extracted from level 4 products and PAR data were extracted from level 2 products, with a 30 min interval, in 2007. GPP in Siberia was calculated from net ecosystem exchange (NEE) and air temperature data, with a 30 min interval, from 2004 to 2007. Details of the GPP calculation are provided in Appendix A. The processing of flux data from the United States (US-Ses, US-Wjs, and US-Los), Canada (CA-Let), Japan (JP-TKY, JP-TMK, and JP-MSE), and Thailand (TH-SKR) and the LRC parameters used in this study are described in Thanyapraneedkul et al. (2012), Mineshita et al. (2016), and Muramatsu et al. (2017).

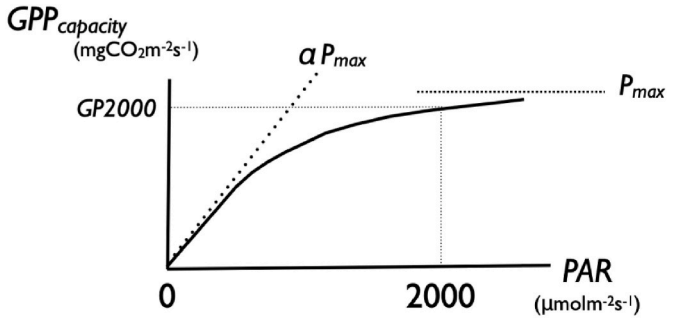

Fig. 2. Light response curve of gross primary production capacity (GPP capacity).

2.2.1. Satellite data

To determine the relationships between the LRC parameters and vegetation indices, MODIS surface reflectance data (MOD09A1) for the same year as the flux data were obtained from the MODIS Land Products Subsets project website (ORNL DAAC, 2008). Data for the period of 2000–2015 were used to determine the selection criteria for pure pixels. The MOD09A1 product has a spatial resolution of 500 m every 8 days, with correction for the effects of scattering and absorption by atmospheric components and aerosols using the transmission, reflectance, and spherical albedo of gas molecules and aerosols (Vermote et al., 2002). The MODIS bands used in this study are shown in Table 2.

The MODIS GPP product (MOD17A2H) (Running et al., 2015) data for newly added flux sites (ES-Agu, FR-Hes, RU-YLF, NL-Loo, IT-Lav, RU-YPF, and FR-Pue) were obtained for the same time period. This product has a spatial resolution of 500 m every 8 days and the data are expressed in units of kg C m^{-2}.

2.3. Data preprocessing for the newly added GHG-Europe and Siberia flux sites

2.3.1. Selection of clear and pure MODIS pixels for vegetation index calculation and CI_{green} calculation at flux sites

MODIS data from 2000 to 2015 for GHG-Europe sites were used to determine the criteria for selecting clear and pure pixels in the MODIS reflectance data. Four pixels from different positions at each site were examined. Because of the uniformity of the land cover, it was considered acceptable to use only four pixels in this study, despite nine pixels (one pixel corresponding to the site position, and eight pixels surrounding the center pixel) having been used in a previous study of a paddy site (Muramatsu et al., 2017). To minimize the effects of clouds, cloud shadows, and aerosols, surface reflectance data were used with MOD35 cloud regions recorded as 00, cloud shadows as 0, aerosol amounts as 00 and 01, and cirrus as 00. However, some contamination remained in the form of thin clouds. To select clear and pure pixels, we used satellite data with blue and 1.2 μm reflectance, and the band ratio of the blue and red reflectance within three standard deviations of the 16-year mean (Table 3), in accordance with Muramatsu et al. (2017).

CI_{green} was calculated every 16 days from the reflectance of a pixel corresponding to the flux site location. If the data were available every 8 days, the average of two values was used. If only one value was available for 16 days, that value was used. If no data were available for 16 days because the selection criteria for clear and pure pixels were not met, that day was treated as missing data.

2.3.2. Selection of GPP under low-stress VPD conditions

A high VPD causes a decrease in the rate of photosynthesis during the day (Pathre et al., 1998; Thanyapraneedkul et al., 2012; Mineshita et al., 2016). In this study, low-stress GPP data corresponding to the period before and after the midday depression of GPP were selected. To determine the threshold for VPD, diurnal variation in GPP, PAR, and VPD was examined every 30 min, and the VPD value at the start of the

Table 1
Flux site descriptions: IGBP class; OSH: Open shrubland, SAV: Savanna, GRA: Grassland, CRO: Cropland, DBF: Deciduous broadleaf forest, CSH: Closed shrubland, WET: Permanent wetland, DNF: Deciduous needleleaf forest, ENF: Evergreen needleleaf forest, EBF: Evergreen broadleaf forest. The symbol * in site ID shows newly added data; and the symbols ⋄, ○ and ♯ shows previous study data in Thanyapraneedkul et al. (2012), Mineshita et al. (2016), and Muramatsu et al. (2017), respectively.

IGBP class	Site ID (This study)	Data year	Name and Country	Location	Annual temp. (C)	Annual precip. (mm)	Dominant Species	Canopy height(m)	Reference
OSH	ES-Agu*	2007	Balsa Blanca, Spain	36.9406°N 2.0329°W	18.0	220	*Machrocloa tenacissima*	1	López-Ballesteros et al. (2016) López-Ballesteros et al. (2018)
OSH	US-Ses○	2007	Sevilleta shrubland, USA	34.3349°N 106.7442°W	13.7	273	*Larrea tridentata, Bouteloua eriopoda*	0.75	Anderson-Teixeira et al. (2011)
SAV	US-Wjs○	2007	Willard Juniper, Savannah, USA	34.4255°N 105.862°W	15.2	361	*Juniperus monosperma, Bouteloua gracilis*	2	Anderson-Teixeira et al. (2011)
GRA	CA-Let○	2003	Alberta-Mixed Grass, Prairie, Canada	49.709°N 112.940°W	5.4	398	*Agropyron dasystachyum A. smithii*	0.317 ± 0.074 (2001–2006)	(Flanagan and Adkinson, 2011)
CRO	JP-MSE♯	2001-2004	Mase paddy, Japan	36.054°N 136.054°E	13.7	1200	rice (*Oryza sativa*)	1.2 (max.)	Ono et al. (2013)
DBF	FR-Hes*	2007	Hess, France	48.6742°N 7.0656°E	9.2	820	Beech (*Fagus sylvatica* L.)	13	Granier et al. (2008)
DBF	JP-TKY○	2003	Takayama, Japan	36.146°N 37.423°E	6.4	2293.5	*Betula ermanii Quercus crispula*	15–20	(Saigusa et al., 2002) Hirata et al. (2008)
CSH (WET)	US-Los○	2007	Lost Creek, USA	46.0827°N 89.9792°W	4.1	828	Alder (*Alnus incana*) Willow *(Salix)*	2	(US-Los site's web page; Sulman et al., 2009)
DNF	RU-YLF*	2004-2007	Spasskaya Pad, Yakutsk, Russia	62.255°N 129.241389 °E	−10.0 (1961–1990)	236.9 (1961–1990)	Dahurica larch (*Larix cajanderi*)	18	Ohta et al. (2008)
DNF	JP-TMK○	2003	Tomakomai, Japan	42.737°N 141.519°E	6.2	1043	Japanese larch *(Larix kaempferi)*	15	(Hirata et al., 2007, 2008)
ENF	NL-Loo*	2007	Loobos, Netherlands	52.1679°N 5.7440°E	9.8	786	Scots pine (*Pinus sylverstris*)	15.1 (1977)	Dolman et al. (2002)
ENF	IT-Lav*	2007	Lavarone, Italy	45.9553°N 11.2812°E	7.0	1150	Fir *Abies alba* (70%)	33–36	Marcolla et al. (2003)
ENF	RU-YPF*	2004-2007	Spasskaya Pad, Yakutsk, Russia	62.241389°N 129.650556°E	−10.0 (1961–1990)	236.9 (1961–1990)	Pine (*Pinus sylvestris*)	10	(Matsumoto et al., 2005)
ENF	JP-FJY○	2003	Fujiyoshida, Japan	35.454°N 138.762°E	10.1	1483	Japanese red pine *(Pinus densiflora)*	20	(Mizoguchi et al., 2012) Hirata et al. (2008)
EBF	FR-Pue*	2007	Puechabon, France	43.7414°N 3.5958°E	10.4	1230	Holm oak (*Quercus ilex L*)	6	Soudani et al. (2014)
EBF	TH-SHR○	2003	Sakaerat, Thailand	14.492°N 101.916°E	24.1	1200–1300	*Hopea ferrea pierre*	35	(Aguilos et al., 2007) Hirata et al. (2008)

Table 2
MODIS bands and bandwidths used in this study.

Band	Bandwidth (nm)	Notation in this study
3	459–479	blue
4	545–565	red
1	620–670	green
2	841–876	NIR
5	1230–1250	1.2 μm

Table 3
Spectral reflectance (R) in the blue and 1.2 μm bands, and ratio of blue and red reflectance.

Spectral reflectance or band ratio	Mean	Standard deviation
R_{blue}	0.041	0.013
$R_{1.2\mu m}$	0.218	0.067
R_{blue}/R_{red}	0.505	0.053

diurnal depression in GPP was used as the threshold value. Data every 30 min with VPD values lower than the VPD threshold were selected to determine the parameters of the LRC for GPP capacity. In previous studies (Thanyapraneedkul et al., 2012; Mineshita et al., 2016; Muramatsu et al., 2017), the VPD threshold was determined to be 1.5 (kPa) for open shrubland (US-Ses) and savanna (US-Wjs), and 2.0 (kPa) for grassland (CA-Let), rice paddy (JP-MSE), wetland (US-Los), deciduous broadleaf forest (JP-TKY), evergreen needleleaf forest (JP-FJY), and evergreen broadleaf forest (TH-SKR). For the GHG-Europe flux sites and Siberia flux sites, it was 0.8 for open shrubland (ES-Agu) and 1.5 (kPa) for the others. Although it is ideal to use a unified VPD threshold for all sites, the conditions under which a decrease in GPP occurred without a decrease in PAR differed among vegetation types.

2.3.3. Parameters of the LRC for the GPP capacity estimation algorithm of the GHG-Europe and Siberia flux sites

To determine the two parameters α and P_{max} in Equation (2), flux data were first fitted to Equation (2) for every 16-day period using a least-squares method, which corresponded to the MODIS satellite observations. Then, α values with a fitting error of less than 35% were averaged (α_{ave}), corresponding to the data during the growing season. Second, Equation (2) was re-fitted using α_{ave} to determine P_{max} for each 16-day period. Third, GP2000 for each 16-day period was calculated by substituting PAR = 2000 (μmol m^{-2} s^{-1}), α_{ave}, and P_{max} into Equation (2). To characterize the differences in LRC parameters, α_{ave}, seasonal changes in P_{max}, and the seasonal value ranges in $\alpha_{ave}P_{max}$ were compared for various vegetation types using the results from the newly added data and data from previous studies (Table 1).

2.4. Comparison of the relationship between GP2000 and CI_{green} for various vegetation types

The relationship between CI_{green} from MODIS and GP2000 for various vegetation types were compared using the results from the flux sites listed in Table 1, and the relationship in Equation (3) was determined for every vegetation type. Next, the linear relationship in Equation (3) for the newly added data was evaluated using a cross-validation method. The flux data were divided into two groups to include seasonal changes equally. Flux data were sequentially numbered every 16 days corresponding to the MODIS observation dates, and the sequential number was divided by 2 for Group 1 if the remainder was 0 and Group 2 if the remainder was 1. For Group 1 and 2, the α_{ave} and P_{max} of the LRCs for every 16-day period were calculated using flux data, GP2000 was calculated from an LRC with the calculated parameters, and the relationship between MODIS CI_{green} and GP2000 was determined. The CI_{green} value of one group (Group1/2) was substituted into the relationship between the other group (Group 2/1). For the evergreen needleleaf forest at NL-Loo, IT-Lav, and RU-YPF, NL-Loo and IT-Lav were divided into two data groups using the remaining sequential numbers, while RU-YPF was divided into two data groups, one for 2004 and 2006 and the other for 2005 and 2007.

2.5. Comparison of the GPP/GPP capacity ratio at the canopy level for various vegetation types

Next, the GPP capacity at the canopy level was calculated using the LRCs. The seasonal variation in the GPP/GPP capacity ratio, and the annual value of the ratio, i.e., the ratio between the annual GPP and the annual GPP capacity at the canopy level were compared for various vegetation types using the results from the GHG-Europe, Ameri-Flux, and AsiaFlux sites.

2.6. Daily and diurnal variation in GPP capacity from MODIS C_{Igreen} for newly added flux sites

Daily and diurnal variation in GPP capacity at the satellite level were calculated using Equation (2) for the newly added flux sites. After estimating GP2000 from MODI CI_{green}, P_{max} was calculated as follows:

$$P_{max} = (GP2000 \times (1 + \alpha_{ave} \times 2000)) / (\alpha_{ave} \times 2000) \quad (6)$$

Then the estimated GPP capacity values from CI_{green} were compared to the Flux GPP and MODIS GPP products.

3. Results

3.1. LRC parameters of GPP capacity

The LRC parameters of α_{ave} in Equation (2) for all data in Table 1 are shown in Fig. 3. The values ranged from 0.0006 to 0.0046, with no clearly characteristic values applicable to every vegetation type. The standard deviation was largest at the Russian site. The P_{max} values every 16 days exhibited seasonal changes as shown in Fig. 4. These differed for open shrub and savanna. At the Es-Agu site, a maximum value of approximately 0.3 was obtained in winter, with low values in summer, which is a dry season with high temperatures. Clear seasonal changes in P_{max} were observed in herbaceous plants in grassland, rice paddy, closed shrubland (permanent wetland), and deciduous broadleaf forests, with maximum values of 1, 2.4, 1.1, and 1.6, respectively. Seasonal changes were also observed in deciduous needleleaf forests. The dominant species at both sites was larch, but the maximum values differed between Japan (JP-TMK) and Siberia (RU-YLF). The maximum value was highest (~2.5) at JP-TMK. In evergreen needleleaf forests, P_{max} exhibited slight

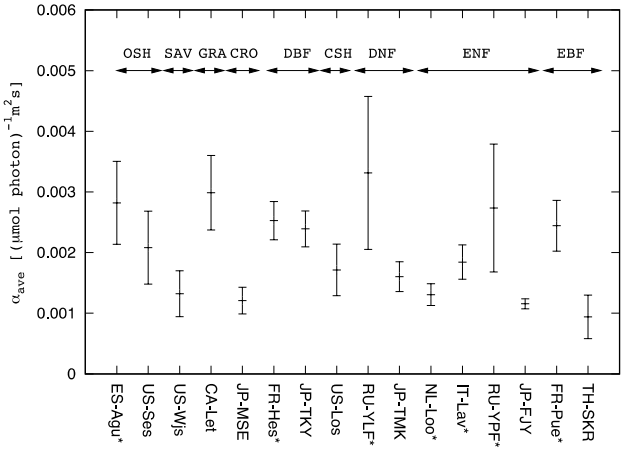

Fig. 3. Mean and standard deviation of the GPP capacity LRC parameters for α_{ave} at 16 sites.

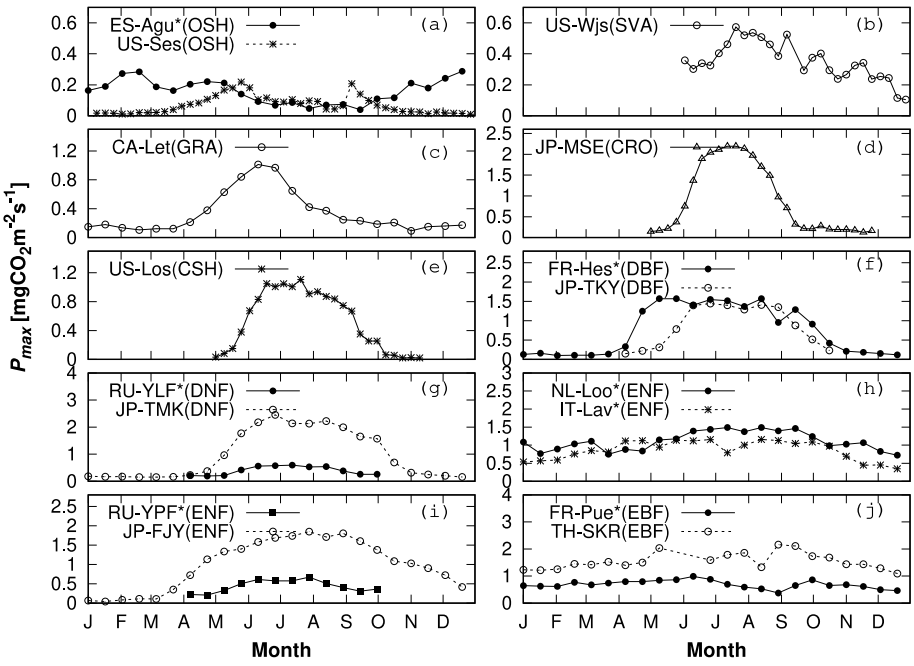

Fig. 4. Seasonal changes in P_{max} for (a) open shrubland (OSH), (b) savanna (SVA), (c) grassland (GRA) (d) cropland (CRO) rice paddy, average value over 4 years, (e) closed shrubland (CSH) in a permanent wetland, (f) deciduous broadleaf forest (DBF), (g) deciduous needleleaf forest (DNF), RU-YLF, average value over 4 years, (h, i) evergreen needleleaf forest (ENF), RU-YPF, average value over 4 years, and (j) evergreen broadleaf forest (EBF).

seasonal changes, except at JP-FJY. The *Pinus densiflora* forests at JP-FJY exhibited clear seasonal changes, with a change in leaf color from green to yellow evident in photographs taken on October 11 and October 31, 2007, respectively. In evergreen broadleaf forests, the maximum values were lower in Europe (FR-Pue) than in tropical areas (TH-SKR). Seasonal values of P_{max} could be converted into GP2000 by substituting $PAR(t) = 2000$ into Equation (2), and the seasonal changes in GP2000 are shown in Appendix B.

Fig. 5 shows the average and the range of seasonal changes in terms of the minimum and maximum values during the growing season from the initial slope of the LRC in Equation (2) of $\alpha_{ave}P_{max}$. The average values were 0.0003–0.002. The smallest values were for open shrubland and savanna, followed by grass and cropland (rice paddy). For closed shrubland (in a permanent wetland), deciduous broadleaf, deciduous needleleaf, evergreen needleleaf, and evergreen broadleaf forests, the average values were 0.001–0.002; the highest value recorded was in deciduous broadleaf forest, which also had the largest range of seasonal change. Evergreen forests also displayed seasonal changes in the initial slope, with particularly large changes in the *P. densiflora* forests at the JP-FJY site.

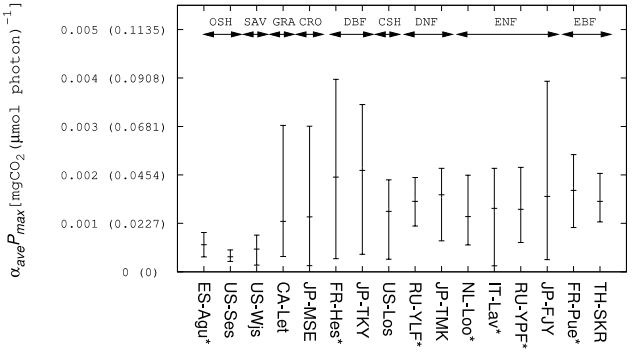

Fig. 5. Average and seasonal range of initial slope of the LRC at 16 sites. The $\alpha_{ave}P_{max}$ value is shown in $mgCO_2$ (μmol photon)$^{-1}$. The value converted into $molCO_2$ (mol photon)$^{-1}$, which is frequently used in the field of plant physiology, is shown in parentheses on the vertical axis.

3.2. Relationship between CI_{green} and GP2000

The relationship between CI_{green} and GP2000 was investigated for newly added data and data from previous studies for various vegetation types. The data are summarized in Table 4 and illustrated in Fig. 6. For open shrubland, savanna, grassland, and cropland (rice paddy), the data displayed a linear relationship. The newly added ES-Agu site data were also distributed near the regression line. For deciduous broadleaf forests and permanent wetland there was a linear relationship. Deciduous broadleaf *Fagus sylvatica* forests in France (FR-Hes) and *Betula ermanii* and *Quercus crispula* forests in Japan (JP-TKY) exhibited a similar distribution of hysteresis. The slope was lower for DBF and CSH (Fig. 6(b)) than for OSH, GRS, and CRO (Fig. 6(a)). The US-Los site was in closed shrubland (permanent wetland) and had a different vegetation type. Nevertheless, the relationship between CI_{green} and GP2000 at this site was similar to that of deciduous broadleaf forests. This site had seasonal variation in GP2000 and P_{max}, but the degree of variation was less than that in broadleaf forests. These characteristics were also observed in the relationship between CI_{green} and GP2000. In the *P. densiflora* forests of JP-FJY, there were 4-fold (2–6-fold) seasonal changes in CI_{green} over 1 year due to the change in leaf color, which was recorded as described in the previous section. The slope of the relationship was the same as that for deciduous broadleaf forests. The range of CI_{green} values at the NL-Loo and RU-YPF sites were lower than that at JP-FJY. Mixed forests in which evergreen needleleaf trees accounted for more than 70%, such as those at IT-Lav, had a range of CI_{green} values similar to those observed at JP-FJY, but the data points were widely distributed. For the evergreen broadleaf forests, the magnitudes of changes in CI_{green} and GP2000 over 1 year were small at 2- and 0.5-fold, respectively. Although there was no relationship between CI_{green} and GP2000 at each site, the slope of the linear regression for the relationship between the two sites was the same as that between deciduous broadleaf forest and evergreen needleleaf forest within a small range of error.

The highest slope value (0.40) was obtained for open shrubland,

Table 4
Relationship between GP2000 and CI_{green} for each vegetation type.

Vegetation types (IGBP class) (IGBP class)	*GP2000*			No. of data	*GP2000* = aCI_{green} + b		RMSE	R^2	p
	min.	max.	ave.		a	b			
Open shrubland (OSH) Savanna (SVA) Grasslands (GRA) Croplands (CRO)	0.01	1.57	0.36	123	0.4 ± 0.01	−0.28 ± 0.02	0.11	0.94	<0.001
Deciduous broadleaf forest (DBF) Closed shrubland (CSH)	0.02	1.32	0.58	49	0.17 ± 0.01	−0.34 ± 0.07	0.19	0.81	<0.001
Deciduous needleleaf forest (DNF)	0.16	1.66	0.52	45	0.24 ± 0.01	−0.31 ± 0.05	0.14	0.87	<0.001
Red pine of JP-FJY (ENF)	0.51	1.26	0.96	9	0.18 ± 0.04	0.15 ± 0.18	0.11	0.76	0.002
Evergreen needleleaf forest (ENF)	0.21	1.08	0.63	65	0.15 ± 0.02	0.03 ± 0.07	0.17	0.54	<0.001
Evergreen broadleaf forest (EBF)	0.32	1.37	0.73	27	0.16 ± 0.03	−0.09 ± 0.17	0.18	0.51	<0.001

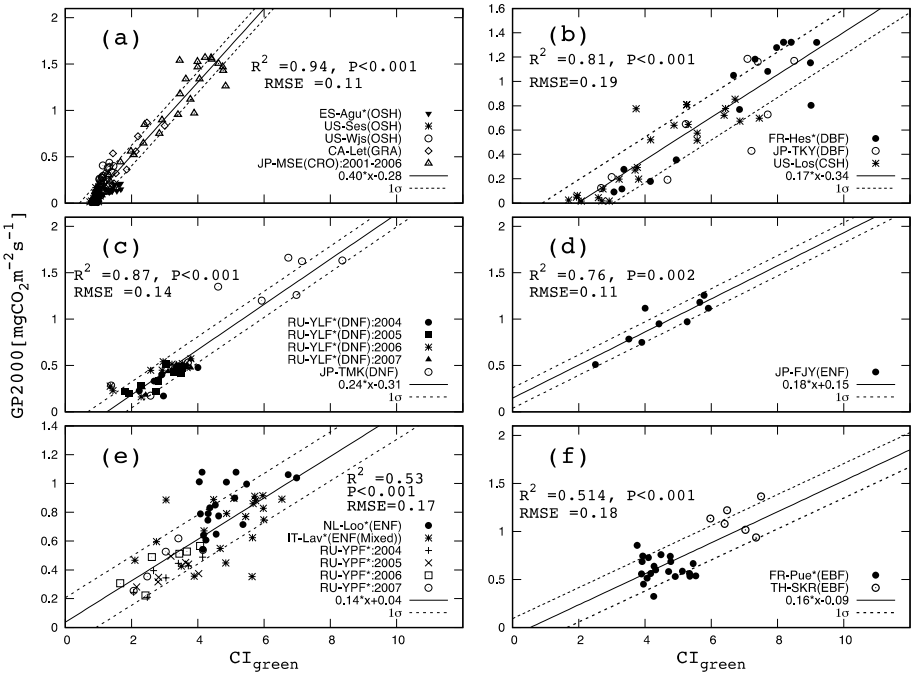

Fig. 6. Relationship between CI_{green} and GP2000 for (a) open shrubland (OSH), savanna (SAV), grassland (GRA), and cropland (CRO) rice paddy (JP-MSE), (b) deciduous broadleaf forest (DBF) and closed shrubland (CSH) in a permanent wetland, (c) deciduous needleleaf forest (DNF), (d) evergreen needleleaf forest (ENF) of *Pinus densiflora* in JP-FJY, (e) ENF except JP-FJY, and (f) evergreen broadleaf forest (EBF). Solid and dashed lines represent linear regression fitting results and their one sigma values; asterisks (*) indicate data newly added in this study.

savanna, and cropland (rice paddy). The next highest value was obtained for deciduous needleleaf forest (0.24), and similar slopes in the range of 0.15–0.18 were obtained for the other vegetation types, i.e., deciduous broadleaf forest, closed shrubland, evergreen needleleaf forest, and evergreen broadleaf forest. The intercept of Equation (3) tended to have a negative value for deciduous vegetation types and a value close to zero for evergreen vegetation types.

The results of the cross-validation are shown in Fig. 7. For ES-Agu, the GPP capacity estimated from the linear relationship in Equation (3) was higher than the Flux GPP. For the other sites, estimates were distributed near the 1:1 line. The root mean square error (RMSE) values for OSH, DBF, DNF, ENF, and EBF were 0.07, 0.07, 0.02, 0.005, and 0.07, respectively.

3.3. The GPP/GPP capacity ratio based on flux data

The seasonal variation in the GPP/GPP capacity ratio of evergreen needleleaf forests was stable over the year, and the yearly value of the ratio was higher than 0.94 (Fig. 8). For the other vegetation groups, the tendency of seasonal variation in the ratio was dependent on the site. For evergreen broadleaf forest, the seasonal variation at TH-SKR was stable over the year, with a maximum value of 0.961, but at FR-Pue, it was lower and decreased from July to September. In deciduous needleleaf forests, the seasonal variation in the ratio at RU-YLF was stable over the year, with an annual value of 0.953, whereas at JP-TMK, it was not stable over time and the annual value (0.680) was lower than that at RU-YLF. For deciduous broadleaf forest and wetland, there was slight seasonal variation. The ratio decreased slightly from June in the growing season. For the rice paddy site at JP-MSE, the ratio was stable, with an annual value of 0.917. The annual value for open shrubland was lower than those of all forest types, except at JP-TMK. There was considerable noise in the ratio, which was higher than in the ratio for open shrubland when GPP was lower than 1 $gCO_2m^{-2}day^{-1}$. The use of this method was considered to be limited when GPP was low. For sites with a stable ratio close to one, the GPP capacity was considered a first-order approximation of GPP.

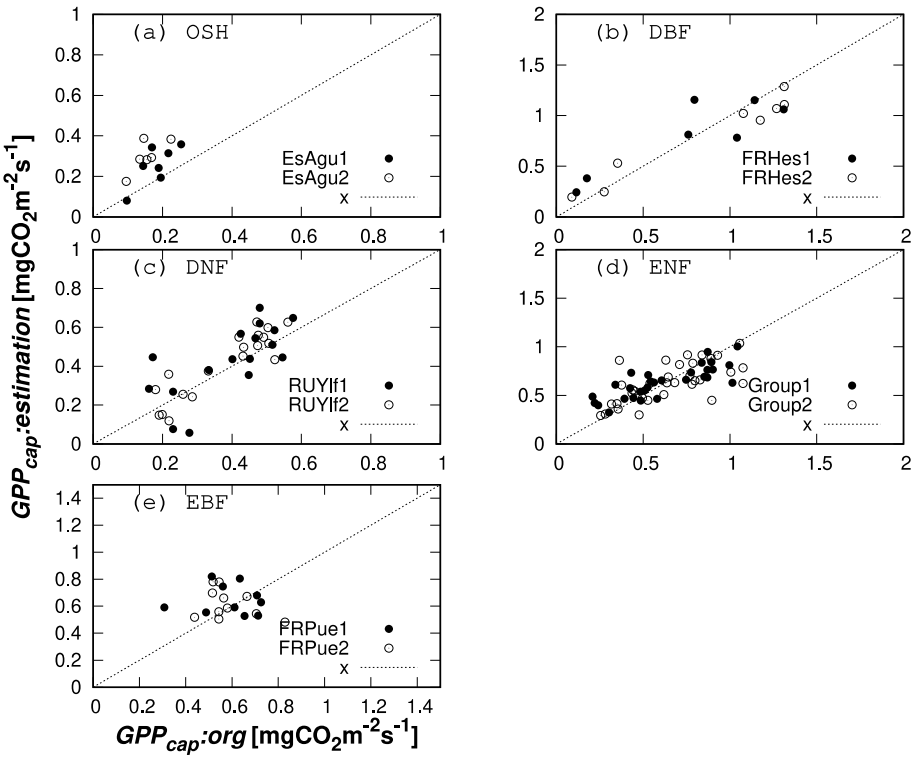

Fig. 7. Cross-validation of linearity in each vegetation group for newly added data. (a) ES-Agu data for open shrubland (OSH), savanna (SAV), and grassland (GRA). (b) FR-Hes1 data for deciduous broadleaf forest (DBF) and closed shrubland (CSH). (c) RU-YLF data for deciduous needleleaf forest (DNF). (d) Half of the NL-Loo, IT-Lav and RU-YPF data, and (e) FR-Pue data for EBF.

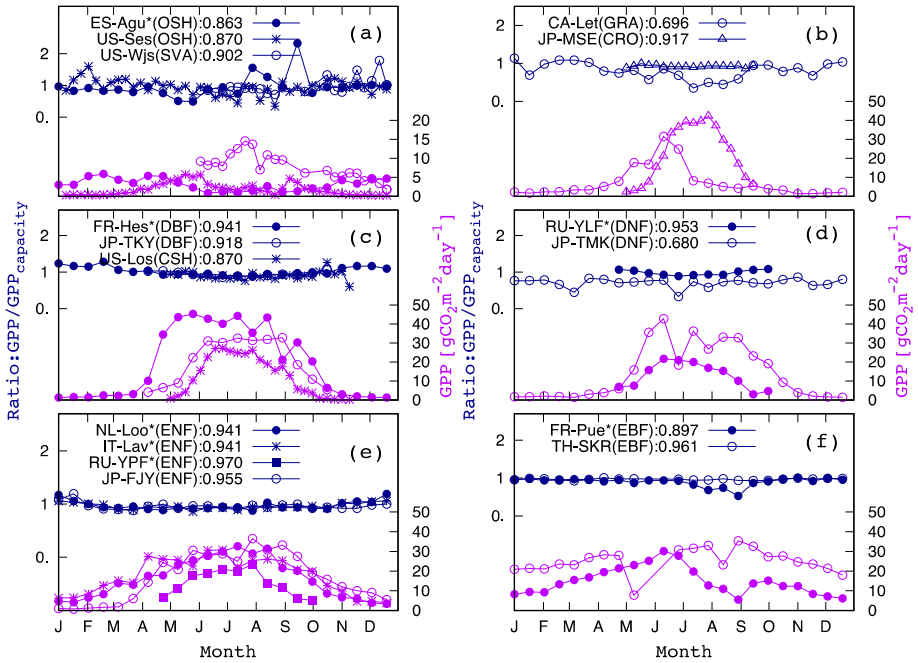

Fig. 8. Seasonal variation of flux data in the daily GPP/GPP capacity ratio (blue) and GPP (pink) for (a) open shrubland (OSH) and savanna (SAV), (b) cropland (CRO) rice paddy and grassland (GRA), (c) deciduous broadleaf forest (DBF) and closed shrubland (CSH) in a permanent wetland, (d) deciduous needleleaf forest (DNF), (e) evergreen needleleaf forest (ENF), and (f) evergreen broadleaf forest (EBF). (For interpretation of the references to color in this figure legend, the reader is referred to the Web version of this article.)

3.4. Daily and diurnal variation in GPP capacity from MODIS C_{Igreen} for the newly added flux sites

Next, we applied our algorithm to satellite data to estimate GPP capacity. The daily GPP capacity from MODIS CI_{green} at the newly added flux locations was compared to the daily Flux GPP and MODIS GPP products (Fig. 9). The capacity estimated from the CI_{green} at ES-Agu was overestimated in winter but reproduced the depression in summer Flux

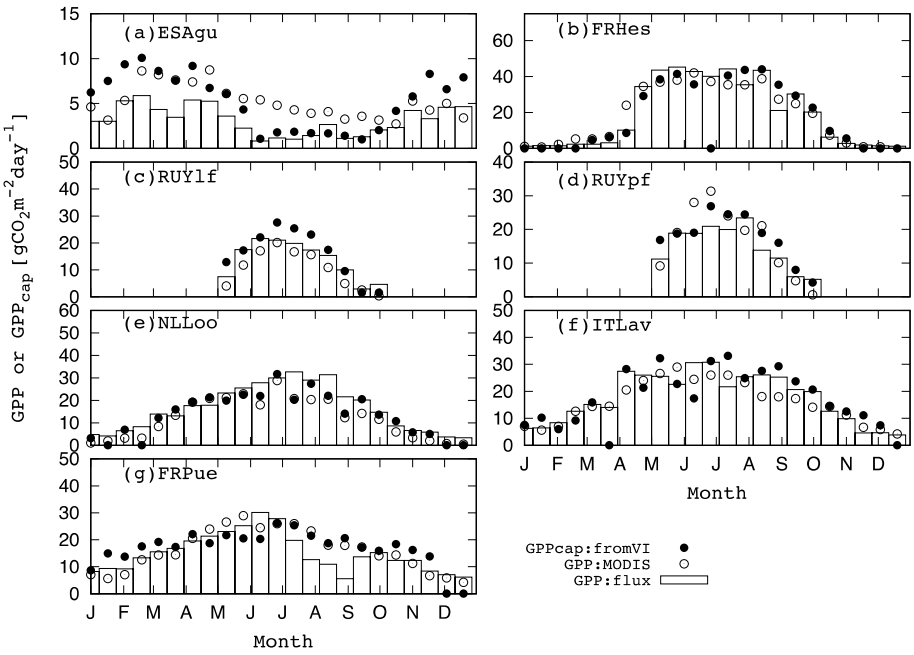

Fig. 9. Daily GPP capacity from the CI_{green}, daily GPP of flux data, and MODIS GPP product for (a) ES-Agu (open shrubland [OSH]), (b) FR-Hes (deciduous broadleaf forest [DBF]), (c) RU-YLF (deciduous needleleaf forest [DNF]), average value for 2004–2007, (d) RU-Ypf (evergreen needleleaf forest [ENF]), average value for 2004–2007, (e) NL-Loo (ENF), (f) IT-Lav (ENF), and (g) FR-Pue (evergreen broadleaf forest [EBF]). CI_{green} was not available in late June for FR-Hes and late May for ITLav.

GPP well. The MODIS GPP product reproduced some of the winter Flux GPP well but not the summer Flux GPP depression. Both the FR-Hes estimates and MODIS GPP product captured the seasonal changes in Flux GPP. The RU-Ylf estimates were higher than the MODIS GPP product, and both approximately captured the seasonal patterns of Flux GPP. Both the RU-Ypf estimates and MODIS GPP product were reproduced well in some months but not in others. The NL-Loo estimate and MODIS GPP product were nearly identical but were lower than the Flux GPP from July to September. The IT-Lav and FR-Pue estimates and the MODIS GPP product were reproduced well in some months but not in others.

One of the key features of the algorithm used in this study was its ability to calculate diurnal changes in the instantaneous GPP capacity using an LRC. Fig. 10 shows examples of the diurnal variation in the instantaneous GPP capacity. An example of the overestimation of the diurnal variation in the instantaneous GPP capacity from MODIS CI_{green} was the ES-Agu site on Mar. 6 (Fig. 10 (a1)), which corresponded to a period when the daily GPP capacity was also overestimated in Fig. 9 (a). Conversely, another example at ES-Agu on May 9 (Fig. 10 (a2)), showed that the GPP capacity was slightly higher than the Flux GPP capacity, but was estimated well. The GPP capacity of Flux and from MODIS CI_{green} were nearly identical during the early morning and late afternoon. The midday depression of photosynthesis, which is the drop from the GPP capacity, was observed around noon in GPP. The GPP capacities from MODIS CI_{green} were slightly higher or lower than the Flux GPP capacity. Midday depressions in Flux GPP were also observed at NL-Loo in April and FR-Pue in July.

4. Discussion

4.1. Initial slope of the LRC parameters derived from flux data

At the leaf level, the initial slope of the LRC is the apparent quantum efficiency, which is related to the total leaf chlorophyll content. The initial slope αP_{max} for the GPP capacity in Equation (2) showed the seasonal variation (Fig. 5) at the canopy level; P_{max} caused the seasonal variation. GP2000 convertible to P_{max} had a linear relationship with CI_{green}, which is correlated with chlorophyll content, as seasonal changes in αP_{max} for GPP capacity are considered to be related to seasonal changes in canopy chlorophyll content. Previous studies of the net ecosystem exchange (NEE) that did not focus on unstress conditions reported the similar results, *i.e.*, the initial slope (Q in Equation (5)) of the LRC showed seasonal variation and was similar to that of P_{max} in a temperate mixed forest (Zhang et al., 2006); sagebrush steppe, short grass steppe, and mixed grass prairie (Polly et al., 2009); and semi-arid grassland (You et al., 2022). Q and P_{max} have a linear relationship in various biome types, including ENF, EBF, MF (mixed Forest), GRS, SVN, and TND (tundra) (Saito et al., 2009). The initial slope Q in Equation (5) equals αP_{max} in Equation (2), as seasonal changes in P_{max} cause similar seasonal patterns and there is a linear relationship between the two parameters.

The units of α and α_{ave} is the inverse of the incident photosynthetic photon flux density (PPFD), and it was hypothesized that $1/\alpha_{ave}$ represents the light environment. In evergreen broadleaf forest, $1/\alpha_{ave}$ values were higher at TH-SKR than at FR-Pue, with the latitude of TH-SKR being lower than that of FR-Pue. Regarding the evergreen needle leaf and deciduous needle leaf types, the high-latitude sites RU-YPF and RU-YLF had the lowest $1/\alpha_{ave}$ values for the same plant types. Lin et al. (2024) showed that the initial slope (α_{ave} P_{max} in this study) tended to decrease with increasing latitude, with P_{max} varying weakly with latitude for 64 typical ecosystems of ChinaFLUX ecosystem measurements over 20 years. Our results showed a similar decrease in α_{ave} (increasing as $1/\alpha_{ave}$) with increasing latitude. However, not all of the differences in $1/\alpha_{ave}$ values could be explained based only on the latitude of the sites. For example, at site NL-Loo, the latitude was slightly higher, but the value of $1/\alpha_{ave}$ was not as low as those expected ranges. This was likely due to the fact that plants in NL-Loo gather light for optimal photosynthesis than plants at the same latitude. Additionally, the topography around this location is less undulating. One possible reason for these differences is that Equation (2) used the incident PPFD (not absorbed PPFD) because $1/\alpha_{ave}$ values would be affected by leaf angles. The leaf angle could be a critical parameter for plants to achieve optimal photosynthesis performance (Yang et al., 2023). For example, if the leaf angle is perpendicular to sunlight, more light is available. On the other

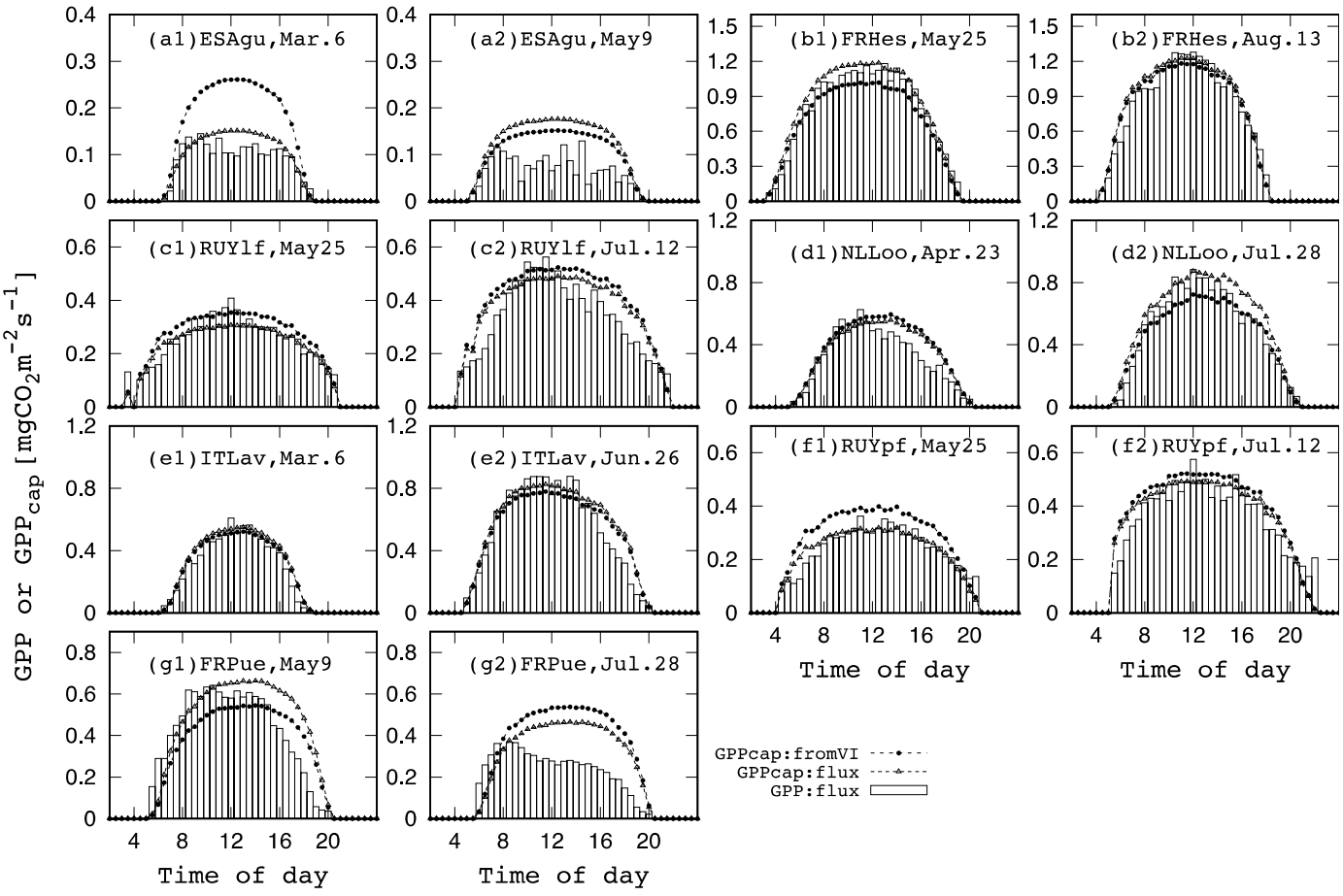

Fig. 10. Diurnal variation in the instantaneous GPP capacity from MODIS CI_{green} and from Flux data, and in Flux GPP for (a1, 2) ES-Agu (open shrubland [OSH]), (b1, 2) FR-Hes (deciduous broadleaf forest [DBF]), (c1−2) RU-Ylf (deciduous needleleaf forest [DNF]), (d1, 2) NL-Loo (evergreen needleleaf forest [ENF]), (e1, e2) T-Lav (ENF), (f1−f2) RU-Ypf (ENF), and (g1, 2) FR-Pue (evergreen broadleaf forest [EBF]).

hand, if the leaf angle is steeper, more light is not available, but irradiation light can be reduced to maximize carbon gain (Falster and Westoby, 2003). Furthermore, plants adjust leaf angles over the short or long term in response to environmental and biological drivers (Yang et al., 2023). Thus $1/\alpha_{ave}$ may differ from the values expected based on latitude because leaf angles can be adjusted to collect appropriate light within the canopy. Further studies using other flux sites are needed to confirm this hypothesis.

4.2. *Relationship between CI_{green} and GP2000*

The liner relationship between GP2000 and CI_{green} for the newly added data was similar for the same vegetation type, even though the continents were different. The relationship between them showed hysteresis, particularly in deciduous broadleaf forests, as shown in Fig. 6. The reason for focusing on the linear relationship between the two parameters is that there may have been pixels that were not occupied by uniform vegetation cover. A nonlinear relationship increases the uncertainty of estimations in heterogeneous pixels.

The Farquhar photosynthesis model parameters (Farquhar et al., 1980) of the potential electron transport rate (J_{max}) and maximum carboxylation rate (V_{Cmax}) have strong linear correlations with leaf chlorophyll content in leaves (Wullschleger, 1993). This is because plants optimize their resource allocation to preserve the balance between their enzymatic Rubisco and chlorophyll capabilities (Wullschleger, 1993). Within deciduous forests, V_{Cmax} values have a stronger linear relationship with the chlorophyll content of a canopy than with J_{max} values (Croft et al., 2017). Typically, the J_{max} values are approximately double the V_{Cmax} values (Leuning, 1997; Hikosaka et al., 2007), and seasonal changes in V_{Cmax} values have been shown to regulate P_{max} when the intercellular partial pressure of CO_2 is approximately 20 Pa in canopy leaves (this study was on *Q. crispula* in a cool temperate forest; Hikosaka et al., 2007). Therefore, we believed that GP2000, which is the parameter responsible for high PAR under low-stress conditions, would be limited by V_{Cmax}. There was a strong correlation between V_{Cmax} and chlorophyll content. This was also true for CI_{green} because there was a linear relationship between GP2000 and CI_{green}.

Furthermore, previous studies of NEE including both stressed and non-stressed conditions reported that the interannual variability in P_{max} is positively correlated with LAI (Laurila et al., 2001; Polly et al., 2009; Gilmanov et al., 2010; Zhang et al., 2012; Tong et al., 2014; You et al., 2022). From the perspective of photosynthesis processes, changes in LAI imply changes in canopy chlorophyll content. Given the seasonal changes in the canopy chlorophyll content, our assumption that the LRC parameter P_{max} is related to the canopy chlorophyll content under low-stress conditions was considered reasonable.

Hysteresis has been reported in the relationships between the daily P_{max} and vegetation indices based on red-edge wavelength, such as the NDVI, EVI, and CI (Muraoka et al., 2013; Gitelson and Merzlyak, 1994), with the NDVI formula $= (R_{750} - R_{705})/(R_{750} + R_{705})$ in a deciduous broadleaf forest (JP-TKY) (Sims et al., 2002). A curvilinear hysteresis

was observed, particularly from spring to midsummer. By contrast, the canopy chlorophyll index (CCI), which is based on the ratio of the derivative of the red-edge wavelength range ($CCI = D_{715–725}/D_{695–705}$) (Sims et al., 2006), has an almost linear relationship with the daily P_{max} from spring to midsummer and from midsummer to early winter (Muraoka et al., 2013). The seasonal patterns of leaf reflectance of *B. ermanii* and *Q. crispula* at the JP-TKY site indicated a low chlorophyll content, possibly due to carotenoid effects. Young leaves had a higher green reflectance and lower NIR reflectance than mature leaves, with the NIR reflectance reflecting the developmental pattern of the mesophyll structure (Noda et al.). Young thin leaves have a lower NIR reflectance because the mesophyll structure is too underdeveloped. The NIR reflectance of CI_{green} was used as a baseline because it is not sensitive to chlorophyll content. The lower NIR reflectance in young leaves would result in lower CI_{green} values than expected due to the actual chlorophyll content. This lower NIR reflectance in the leaf development period may have caused one-way hysteresis. In a mixed temperate forest, the midday GPP and total chlorophyll content in the canopy (Chl_{canopy}) multiplied by the PAR have a linear relationship mid-season; however, the slope of the relationship was slightly lower in mid-season than at the start or end of the season (Croft et al., 2015). The characteristics of leaf gas exchange vary in the leaf expansion period and in mature leaves (Kosugi and Matsuo, 2006). From the seasonal patterns of the chlorophyll content, the light-saturated photosynthetic rate (i.e., P_{max}), maximum carboxylation rate at 20 °C (V_{Cmax20}), and potential electron transport rate at 20 °C (J_{max20}) for *B. ermanii* and *Q. crispula* in JP-TKY have been determined (Noda et al., 2015). The P_{max} and V_{Cmax20} decreased approximately 10 days earlier than the chlorophyll content and J_{max20} decreased during the senescence period. Considering these previously reported findings, the lower photosynthetic capacity in the leaf senescence period than in the mature leaf period, with the same amount of chlorophyll in both periods, likely caused a one-way hysteresis in the leaf senescence period.

A seasonal change was clearly detected among deciduous plant functional types (PFTs), and the relationship between CI_{green} and GP2000 was determined. By contrast, evergreen PFTs have green leaves throughout the year, and the ranges of CI_{green} and GP2000 were not large, except at JP-FJY, where a change in leaf color was observed. For the small ranges of CI_{green} and GP2000 throughout the year, it was impossible to determine their relationship based on data from only one site. In this study, the CI_{green} and GP2000 distributions of ENF at annual air temperatures of −10 °C to 10 °C showed a broad linear relationship (Fig. 6 (e)).

Theoretically, if CI_{green} represents the chlorophyll content, it should be zero when GP2000 is zero. The zero intercept of the relationship between CI_{green} and GP2000 represents this point in the relationship. A near zero value of the intercept was observed for evergreen vegetation types and a negative value was observed for herbaceous and deciduous vegetation types (Fig. 6). Herbaceous and deciduous vegetation areas have seasons with no green vegetation, resulting in similar spectral reflectances of withered leaves and sometimes soil. CI_{green} was almost 1 when the GP2000 is zero, which means that the R_{NIR}/R_{green} ratio was close to 2. The spectral reflectance of withered leaves and soil at green wavelengths was higher than that of green vegetation, with a R_{NIR}/R_{green} ratio close to 2.

Herbaceous vegetation dominated sites with higher slopes. Herbaceous and woody plants have a different canopy structure and light enters the canopy differently. Peng et al. (2017) analyzed the relationship between the canopy chlorophyll content and a vegetation index for maize and soybean using hyperspectral radiometer data and found that the relationship was the same between crops with different canopy structures under a $CI_{red\text{-}edge}$. Their study of herbaceous crops is one example of the response of a vegetation index to vegetation under different canopy structures. The $CI_{red\text{-}edg}$ determined with the Sentinel-2/MSI sensor is the most promising candidate for the development of a sensitive index of canopy chlorophyll under different canopy structures. In addition, the relationship between GP2000 and the chlorophyll content of the canopy itself must be studied.

4.3. Estimation of GPP capacity from satellite data and the applicable scope of the model

The proposed approach used LRC to estimate instantaneous GPP capacity and was able to estimate instantaneous GPP capacity on a sub-day scale. The diurnal variation in the instantaneous GPP observed under high stress indicates that the photosynthesis rate increases as increasing light intensity when weather conditions are appropriate for photosynthesis in the morning, then high-stress conditions cause stomata closure and decrease the photosynthesis rate, and after the stress alleviated, the stomata reopen and photosynthesis rates increase again. These phenomena were observed not only at the leaf level (Kamakura et al., 2011, 2012, 2021) but also at the canopy level (Fig. 10 (a1, 2; d1)). The instantaneous GPP capacity on a sub-day scale was calculated from LRC (Fig. 10). The parameter P_{max} was estimated from CI_{green}, and α_{ave} was determined for each vegetation type from the flux data. The instantaneous Flux GPP showed a drop from the instantaneous GPP capacity (Fig. 10 (a1, 2; c2; d1; g1, 2)). From this result, the instantaneous GPP capacity could be considered the baseline of the instantaneous GPP under unstressed condition. Furthermore, the midday depression will be able to be calculated from the area between the baseline and GPP. Thus the baseline of instantaneous GPP at the sub-day scale is important for quantifying midday depression.

The proposed approach used GPP selected under low-stress conditions using atmospheric dryness (VPD) to determine the LRC parameters, although low soil water content (SWC) can affect GPP. There is often a correlation between VPD and SWC, making it difficult to distinguish effects on GPP reduction and canopy-level stomatal conductance. Recently, Liu et al. (2020) reported that soil moisture (SM) dominates dryness stress rather than VPD when studying solar-induced fluorescence as an indicator of GPP with SM and VPD. By contrast, Kimm et al. (2020) reported the results of a path analysis to characterize connections among environmental variation in precipitation, SWC, relative humidity (RH), air temperature (Ta), VPD, and canopy-level stomatal conductance (Gs). SWC affects both RH and Ta, which both determine VPD, which makes a dominant contribution to Gs at hourly and daily scales at AmeriFlux sites, where soybean and corn grow in U.S. Corn Belt. Furthermore Fu et al. (2022) reported that both GPP and Gs had negative sensitivity to increasing VPD across the entire range of SWC at 15 sites major ecosystems sites across Europe over a 5-year period that included extreme summer drought, and showed negative sensitivity to decreasing SWC mainly at a restricted range of low SWC values. Based on these findings, we considered it reasonable to select less water stress data based on VPD at the diurnal scale, as canopy-level stomatal closure responds to increased VPD and VPD reflects decreased SWC.

Vegetation at high latitudes grows under low temperatures. The example of May at the RU-YLF site included a low air temperature in the early morning, as shown in Fig. D1. Early morning leaf and air temperatures were cooler and solar radiation intensity was lower, possibly preventing stomatal opening. This issue must be addressed in future studies.

Lin et al. (2024) reported significant spatial heterogeneity in average LRC parameters during the growing season, varying with plant species and vegetation cover due to geographic variation in environmental factors. CI_{green}, derived from satellite sensor data, was closely linked to canopy chlorophyll content and reflected vegetation cover and density across different regions, indicating its potential to capture plant responses to environmental conditions. In our study, the relationship between CI_{green} and GP2000, which is important for determining the LRC parameter P_{max}, was applicable to the same vegetation groups, even of different continents, which is likely advantageous for obtaining LRC parameters in various geographic regions globally. When estimating the

GPP capacity using this relationship, the estimation error would be larger than that determined at size-restricted sites, as shown in Fig. 7. For a particular region, it would be better to use relationships specific to that region to reduce the estimation error.

Plant responses to climate change are complex due to diurnal weather variation, in addition to regional annual mean variation. The decrease in instantaneous GPP diurnal variation can be considered a plant response to diurnal weather variation. Instantaneous GPP capacity can be considered a baseline that is independent of diurnal drought. It remains unclear whether changes in GPP under climate change depend on those in the baseline or the diurnal decrease in photosynthesis. The proposed approach could be used to examine changes in the GPP baseline using satellite observations; furthermore, it can also be applied under severe stress conditions at sub-daily time scales. For such future applications, the midday depression and instantaneous GPP would be derived using the proposed GPP capacity combined with independent stress factor data. For example, canopy-level stomatal regulation would be measurable using high-frequency thermal sensing data obtained by meteorological satellites, with recently improved spatial resolution.

5. Conclusions

This study investigated the LRC parameters and the relationship between GP2000 and CI_{green} across 16 sites spanning tropical to subarctic climates on the Eurasian and North American continents. The average initial slope of the LRC during the growing season was 0.0003–0.0021 $mgCO_2$ (μmol photon)$^{-1}$. A linear relationship between GP2000 ($mgCO_2\ m^{-2}\ s^{-1}$) related to P_{max} and CI_{green}, which is sensitive to canopy chlorophyll content, was observed in most vegetation types, except for deciduous broadleaf forests, where hysteresis occurred. The relationship was strongest in herbaceous-dominated sites, such as open shrubland, savanna, and cropland, with the slope highest at 0.40. Woody plant sites exhibited lower slopes, with the next highest value of 0.24 found in deciduous needleleaf forests, and values ranging from 0.15 to 0.18 for other vegetation types (deciduous broadleaf forest, evergreen needleleaf forest, evergreen broadleaf forest). The intercept tended to be negative for deciduous vegetation and close to zero for evergreen types.

The yearly GPP/GPP capacity ratio was close to one at the canopy level. When applied to satellite data, the method produced seasonal patterns in daily GPP capacity that were similar with MODIS GPP products and Flux GPP. The diurnal variation in instantaneous GPP capacity showed that under high dryness, Flux GPP decreased around noon but was nearly identical to GPP capacity in the early morning and late afternoon. Instantaneous GPP capacity can be considered a baseline for stress-free conditions, crucial for quantifying midday depression at subday scales.

Further research should focus on developing more sensitive indices, such as those based on the red-edge band or total canopy chlorophyll content. The proposed method has potential applications under severely stressed conditions and at sub-daily time scales. High-frequency thermal sensing data from meteorological satellites with improved spatial resolution could be used to measure canopy-level stomatal regulation, enhancing our understanding of instantaneous GPP under varying environmental stresses.

CRediT authorship contribution statement

Kanako Muramatsu: Writing – review & editing, Writing – original draft, Visualization, Validation, Supervision, Resources, Project administration, Methodology, Investigation, Funding acquisition, Formal analysis, Data curation, Conceptualization. **Emi Yoneda:** Visualization, Validation, Methodology, Investigation, Formal analysis, Data curation. **Noriko Soyama:** Writing – review & editing, Writing – original draft, Visualization, Funding acquisition, Conceptualization. **Ana López-Ballesteros:** Writing – review & editing, Resources, Funding acquisition, Data curation. **Juthasinee Thanyapraneedkul:** Writing – review & editing, Methodology, Data curation.

Declaration of competing interest

The authors declare that they have no known competing financial interests or personal relationships that could have appeared to influence the work reported in this paper.

Data availability

The authors do not have permission to share data.

Acknowledgments

This work was supported in part by JSPS KAKENHI grant (no. 16K00514); Environmental Research Projects from The Sumitomo Foundation grant (no. 193123); a grant for the Global Change Observation Mission (GCOM); nos. ER2GCF108 and ER3GCF107 of the Japan Aerospace Exploration Agency (JAXA); and the organization for the promotion of gender equality at Nara Women's University. MODIS datasets were provided by Land Processes DAAC and flux data were provided by FLUXNET Network of the Asia-Flux, Ameri-Flux, Fluxnet-Canada and GHG-Europe, and Forestry and Forest Products Research Institute Flux Observation Network (FFPRI FluxNet) in Japan. Funding for the Ameri-Flux data resources was provided by the Office of Science of the U.S. Department of Energy. The research leading to these results has received funding from the Seventh Framework Programme of European Community (FP7/2007–2013) under grant agreement no. 244122 GHGEurope. KM thanks A. Ozaki for the preliminary study of RU-YPF and RU-YLF sites that was performed during graduate training. ALB was supported by a Juan de la Cierva-Incorporación postdoctoral contract IJC2020-045630-I funded by MCIN/0041EI/10.13039/501100011033 and by European Union NextGenerationEU/PRTR. We thank the principal investigators and researchers of the EC observations for providing data and site information: L. Flanagan (CA-Let), K. Ono (JP-MSE), M. Cuntz (FR-Hes), M. Litvak (US-Ses, US-Wjs), S. Murayama (JP-TKY), A.R. Desai (US-Los), B. Kruijt (NL-Loo), (IT-Lav), A. Kotani (RU-YPF and RU-YLF), Y. Mizoguchi (JP-FJY), J. Limousin (FR-Pue), T. Maeda (TH-SKR), and the PI and researchers of JP-TMK and IT-Lav. We also thank the anonymous reviewers for their valuable comments and suggestions.

Appendix A

Based on the flux data from Siberia, GPP was calculated using net ecosystem production (NEP) plus ecosystem respiration (Rec), as follows:

$$GPP(T_{air}) = NEP + Rec(T_{air}) \quad (A.1)$$

Where Rec is plant respiration plus soil respiration as a function of air temperature (T_{air}). The nighttime Rec was calculated as an exponential function of T_{air} to fit nighttime NEP as a function of T_{air} as follows:

$$Rec(T_{air}) = a\exp(bT_{air}) \quad (A.2)$$

Where a and b are empirical constants determined through regression, with b related to the temperature coefficient and the Rec considered at 0 °C. Nighttime data were selected when the friction velocity was higher than 0.2 ms^{-1} and the relative humidity was less than 100% for data with NEP >0. The parameters a and b for the YLF site were 0.068 ± 0.002 and 0.029 ± 0.02, respectively, and those for the YLP site were 0.065 ± 0.002 and 0.039 ± 0.003, respectively.

Appendix B

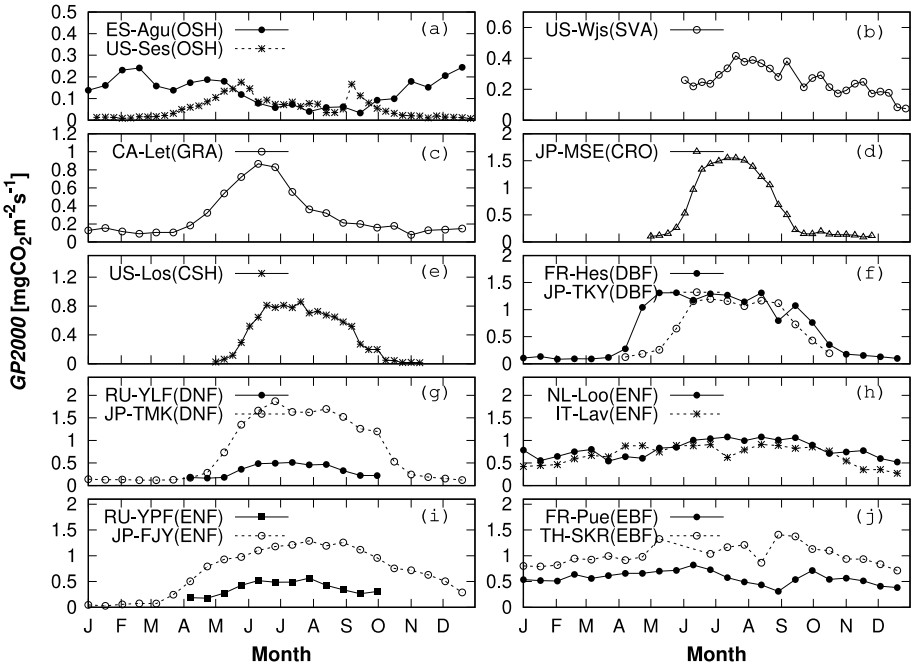

Fig. B1. Seasonal changes in GP2000 for (a) open shrubland (OSH), (b) savanna (SVA), (c) grassland (GRA), (d) cropland (CRO) rice paddy, (e) closed shrubland (CSH) of permanent wetland, (f) deciduous broadleaf forest (DBF), (g) deciduous needleleaf forest (DNF), (h, i) evergreen needleleaf forest (ENF), and (j) evergreen broadleaf forest (EBF).

Appendix C

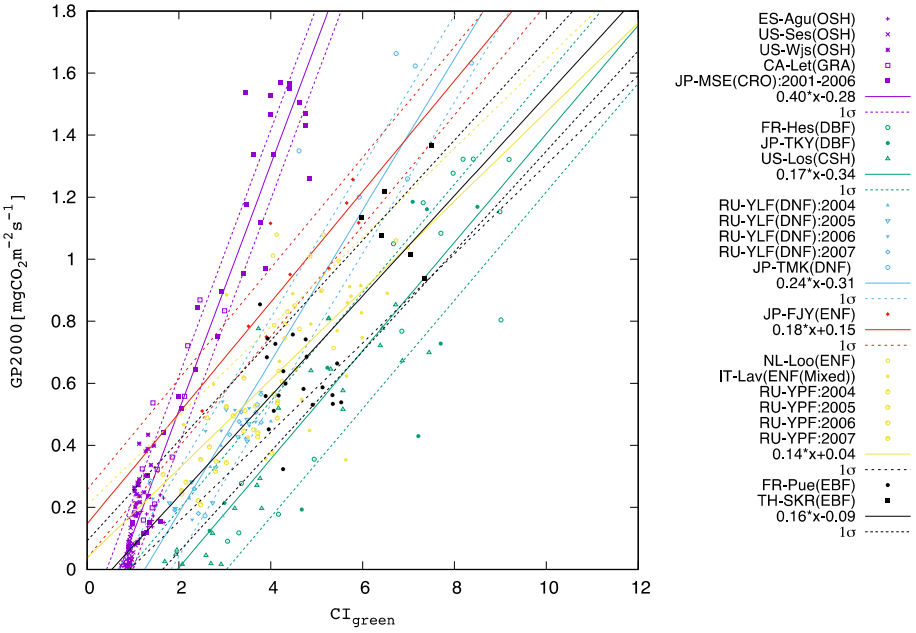

Fig. C1. Relationship between CI_{green} and GP2000 for open shrubland (OSH), savanna (SAV), grassland (GRA), and cropland (CRO) rice paddy (JP-MSE), deciduous broadleaf forest (DBF) and closed shrubland (CSH) in a permanent wetland, deciduous needleleaf forest (DNF), evergreen needleleaf forest (ENF) of *Pinus densiflora* in JP-FJY, and evergreen broadleaf forest (EBF). The solid line represents the fitting results from a linear regression, and the dotted lines indicate the one sigma values for the fitting.

Appendix D

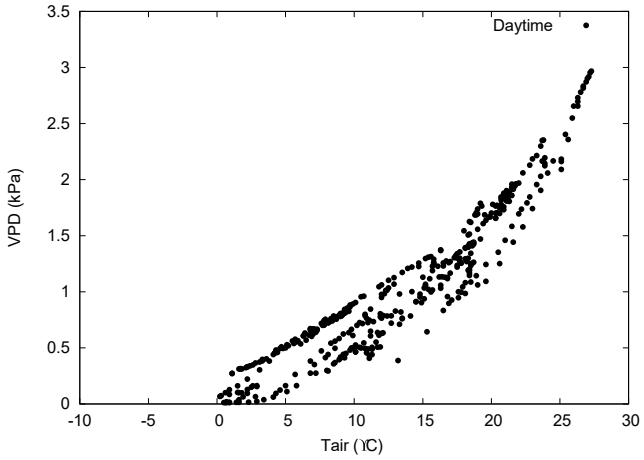

Fig. D1. Air temperature and VPD for 16 days from DOY 145 to 161 at the YLF site.

References

Aguilos, M.M., Gamo, M., Maeda, T., 2007. Carbon budget of some tropical and temperate forest. In: Asia-Flux Newsletter 2007, Special Issue, pp. 18–22.

Anderson-Teixeira, K.J., Delong, J.P., Fox, A.M., Brese, D.A., Litvak, M.E., 2011. Differential responses of production and respiration to temperature and moisture drive the carbon balance across a climatic gradient in New Mexico. Global Change Biol. 17 (1), 410–424. https://doi.org/10.1111/j.13652486.2010.02269.x.

Asner, G.P., Wessman, C.A., Archer, S., 1998. Scale dependence of absorption of photosynthetically active radiation in terrestrial ecosystems. Ecol. Appl. 8 (4), 1003–1021.

Beer, C., Reichstein, M., Tomelleri, E., Ciais, P., Jung, M., Carvalhais, N., Rödenbeck, C., Arain, M.A., Baldocchi, D., Bonan, G.B., Bondeau, A., Cescatti, A., Lasslop, G., Lindroth, A., Lomas, M., Luyssaert, S., Margolis, H., Oleson, K.W., Roupsard, O., Veenendaal, E., Viovy, N., Williams, N., Woodward, F.I., Papale, D., 2010. Terrestrial gross carbon dioxide uptake: global distribution and covariation with climate. Science 329 (5993), 834–838.

Croft, H., Chen, J.M., Froelich, N.J., Chen, B., Staebler, R.M., 2015. Seasonal controls of canopy chlorophyll content on forest carbon uptake: implications for GPP modeling. J. Geophys. Res.: Biogeosciences 10 (1002), 1576–1586.

Croft, H., Chen, J.M., Luo, X., Bartlett, P., Chen, B., Staebler, R., 2017. Leaf chlorophyll content as a proxy for leaf photosynthetic capacity. Global Change Biol. 23, 3513–3524.

Dash, J., Curran, P.J., 2004. The MERIS terrestrial chlorophyll index. Int. J. Rem. Sens. 25 (23), 5403–5413.

Dash, J., Curran, P.J., 2007. Evaluation of the MERIS terrestrial chlorophyll index (MTCI). Adv. Space Res. 39, 100–104.

Dash, J., Curran, P.J., Tallis, M.J., Llewellyn, G.M., Taylor, G., Snoeij, P., 2010. Validating the MERIS Terrestrial Chlorophyll index (MTCI) with ground chlorophyll content data at MERIS spatial resolution. Int. J. Rem. Sens. 31 (20), 5513–5532.

Dolman, A.J., Moors, E.J., Elbers, J.A., 2002. The carbon uptake of a mid-latitude pine forest growing on sandy soil. Agric. For. Meteorol. 111, 157–170.

Falster, D.S., Westoby, M., 2003. Leaf size and angle vary widely across species: what consequences for light interception? New Phytol. 158, 509–525.

Farquhar, G.D., von Caemmerer, S., Berry, J.A., 1980. A biochemical model of photosynthetic CO_2 assimilation in leaves of C3 species. Planta 149, 78–90.

Flanagan, L.B., Adkinson, A.C., 2011. Interacting controls on productivity in a northern Great Plains grassland and implications for response to ENSO events. Global Change Biol. 17, 3293–3311.

Fu, Z., Ciais, P., Prentice, C., Gentine, P., Makowski, D., Bastos, A., Luo, X., Green, J.K., Stoy, P.C., Yang, H., Hajima, T., 2022. Atmospheric dryness reduces photosynthesis along a large range of soil water deficits. Nat. Commun. 13, 989. https://doi.org/10.1038/s41467-022-28652-7.

Furumi, S., Xiong, Y., Fujiwara, N., 2005. Establishment of an algorithm to estimate vegetation photosynthesis by pattern decomposition using multi-spectral data. J. Rem. Sens. Soc. Jpn. 25, 47–59.

Gilmanov, T.G., Aires, L., Belelli, L., Barcza, Z., Baron, V.S., Beringer, J., Billesbach, D., Bonal, D., Bradford, J., Ceschia, E., Cook, D., Corradi, C., Frank, A., Gianelle, D., Gimeno, C., Gruenwald, T., Guo, H., Hanan, N., Haszpra, L., Heilman, J., Jacobs, A., Johnson, D.A., Kiely, G., Li, S.-G., Magliulo, V., Moors, E., Nagy, Z., Nasyrov, M., Owensby, C., Pinter, K., Pio, C., Reichstein, M., Sanz, M.J., Scott, R., Soussana, J.-F., Svejcar, T., Tuba, Z., Zhou, G., 2010. Productivity, respiration, and light-response parameters of world grassland and agro-ecosystems derived from flux-tower measurements. Rangel. Ecol. Manag. 63, 16–39. https://doi.org/10.2111/REM-D-09-00072.1.

Gitelson, A.A., Merzlyak, M.N., 1994. Spectral reflectance changes associated with autumn senescence of *Aesculus hippocastanum* L. and *Acer platanoides* L. leaves. Spectral features and relation to chlorophyll estimation. J. Plant Physiol. 143, 286–292.

Gitelson, A.A., Vina, A., Verma, S.B., Rundquist, D.C., Arkebauer, T.J., Keydan, G., Leavitt, B., Ciganda, V., Burba, G.G., Suyker, A.E., 2006. Relationship between gross primary production and chlorophyll content in crops: implications for the synoptic monitoring of vegetation productivity. J. Geophys. Res. 111, D08S11.

Gitelson, A., Viña, A., Solovchenkoe, A., Arkebauerh, T., Inoue, Y., 2019. Derivation of canopy light absorption coefficient from reflectance spectra. Rem. Sens. Environ. 213, 111276, 1–9.

Granier, A., Bréda, N., Longdoz, B., Gross, P., Ngao, J., 2008. Ten years of fluxes and stand growth in a young beech forest at Hesse, North-eastern France. Ann. For. Sci. 65, 704.

Harazono, Y., Chikamoto, K., Kikkawa, S., Iwata, T., Nishida, N., Ueyama, M., Kitaya, Y., Mano, M., Miyata, A., 2009. Application of MODIS visible band index, greenery ratio to estimate CO_2 budget of a rice paddy in Japan. J. Agric. Meteorol. 65, 365–374.

Harris, A., Dash, J., 2010. The potential of the MERIS Terrestrial Chlorophyll Index for carbon flux estimation. Rem. Sens. Environ. 114, 1856–1862.

Heinsch, F.A., Zhao, M., Running, S.W., Kimball, J.S., Nemani, R.R., Davis, K.J., Bolstad, P.V., Cook, B.D., Desai, A.R., Ricciuto, D.M., Law, B.E., Oechel, W.C., Kwon, H., Luo, H., Wofsy, S.C., Dunn, A.L., Munger, J.W., Baldocchi, D.D., Xu, L., Hollinger, D.Y., Richardson, A.D., Stoy, P.C., Siqueira, M.B.S., Monson, R.K., Burns, S.P., Flanagan, L.B., 2006. Evaluation of remote sensing based terrestrial productivity from MODIS using regional tower eddy flux network observations. IEEE Trans. Geosci. Rem. Sens. 44, 1908–1925.

Hikosaka, K., Nabeshima, E., Hiura, T., 2007. Seasonal changes in the temperature response of photosynthesis in canopy leaves of *Quercus crispula* in a cool-temperature forest. Tree Physiol. 27, 1035–1041.

Hirata, R., Hirano, T., Saigusa, N., Fujinuma, Y., Inukai, K., Kitamori, Y., Yamamoto, S., 2007. Seasonal and interannual variations in carbon dioxide exchange of a temperate larch forest. Agric. For. Meteorol. 147, 110–124.

Hirata, R., Saigusa, N., Yamamoto, S., Ohtani, Y., Ide, R., Asanuma, J., Gamob, M., Hirano, T., Kondo, H., Kosugi, Y., Li, S.G., Nakai, Y., Takagi, K., Tani, M., Wang, H., 2008. Spatial distribution of carbon balance in forest ecosystems across East Asia. Agric. For. Meteorol. 148, 761–774.

Huete, A.R., Liu, H.Q., Batchily, K., van Leeuwen, W., 1997. A comparison of vegetation indices over a global set of TM images for EOS-MODIS. Rem. Sens. Environ. 59 (3), 440–451.

Ide, R., Nakaji, T., Oguma, H., 2010. Assessment of canopy photosynthetic capacity and estimation of GPP by using spectral vegetation indices and the light-response function in a larch forest. Agric. For. Meteorol. 150, 389–398.

Kamakura, M., Kosugi, Y., Tajahashi, S., Matsumoto, K., Okumura, M., Philip, E., 2011. Patchy stomatal behavior during midday depression of leaf CO_2 exchange in tropical trees. Tree Physiol. 31, 160–168.

Kamakura, M., Kosugi, Y., Muramatsu, K., Muraoka, H., 2012. Simulation and observations of patchy stomatal behavior in leaves of *Quercus crispula*, a cool-temperate deciduous broad-leaved tree species. J. Plant Res. 125, 339–349.

Kamakura, M., Kosugi, Y., Takanashi, S., Matsuo, N., Uemura, A., Lion, M., 2021. Temporal fluctuation of patchy stomatal closure in leaves of *Dipterocarpus sublamellatus* at upper canopy in Peninsular Malaysia over the last decade. TROPICS 30 (3), 41–51.

Kimm, H., Guan, K., Gentine, P., Wu, J., Bernacchi, C.J., Sulman, B.N., Griffis, T.J., Lin, C., 2020. Redefining droughts for the U.S. Corn Belt: the dominant role of atmospheric vapor pressure deficit over soil moisture in regulating stomatal behavior of maize and soybean. Agric. For. Meteorol. 287, 107930. https://doi.org/10.1016/j.agrformet.2020.107930.

Kosugi, Y., Matsuo, N., 2006. Seasonal fluctuations and temperature dependence of leaf gas exchange parameters of co-occurring evergreen and deciduous trees in a temperate broad-leaved forest. Tree Physiol. 26, 1173–1184.

Laurila, T., Soegaard, H., Lloyd, C.R., Aurela, M., Tuovinen, J.-P., Nordstroem, C., 2001. Seasonal variations of net CO_2 exchange in European Arctic ecosystems. Theor. Appl. Climatol. 70, 183–201.

Leuning, R., 1997. Scaling to common temperature improves the correlation between the photosynthesis parameters J_{max} and V_{cmax}. J. Exp. Bot. 48 (No. 307), 345–347.

Lin, Y., Chen, Z., Yu, G., Yang, M., Hao, T., Zhu, X., Zhang, W., Han, L., Liu, Z., Ma, L., Dou, X., Luo, W., 2024. Spatial patterns of light response parameters and their regulation on gross primary productivity in China. Agric. For. Meteorol. 345, 109833. https://doi.org/10.1016/j.agrformet.2023.109833.

Liu, L., Gudmundsson, L., Hauser, M., Qin, D., Li, S., Seneviratne, S.I., 2020. Soil moisture dominates dryness stress on ecosystem production globally. Nat. Commun. 11, 4892. https://doi.org/10.1038/s41467-020-18631-1.

López-Ballesteros, A., Serrano-Ortiz, P., Sánchez-Cañete, Oyonarte, C., Pérez-Priego, Ó., 2016. Enhancement of the net CO_2 release of a semiarid grassland in SE Spain by rain pulses. J. Geophys. Res. Biogeosci. 121, 52–66. https://doi.org/10.1002/2015jg003091.

López-Ballesteros, A., Kowalski, A.S., Oyonarte, C., Kowalski, A.S., SerranoOrtiz, P., Sánchez-Cañete, E.P., Moya, M.R., Domingo, F., 2018. Can land degradation drive differences in the C exchange of two similar semiarid ecosystem? Biogeosciences 15, 263–278.

Marcolla, B., Pitacco, A., Cescatti, A., 2003. Canopy architecture and turbulence structure in a coniferous forest. Boundary-Layer Meteorol. 108, 39–59.

Matsumoto, K., Ohta, Tanaka, T., 2005. Dependence of stomatal conductance on leaf chlorophyll concentration and meteorological variables. Agric. For. Meteorol. 132, 44–57.

Mineshita, Y., Muramatsu, K., Soyama, N., Thanyapraneedkul, J., Daigo, M., 2016. Determination of parameters for shrubs in the global gross primary production capacity estimation algorithm. J. Rem. Sens. Soc. Jpn. 3, 236–246.

Mizoguchi, Y., Ohtani, Y., Takannashi, S., Iwata, H., Yasuda, Y., Nakai, U., 2012. Seasonal and interannual variation in net ecosystem production of an evergreen needleleaf forest in Japan. J. For. Res. 17 (3), 283–295.

Monteith, J.L., 1972. Solar radiation and production in tropical ecosystem. J. Appl. Ecol. 9, 747–766.

Muramatsu, K., 2018. Canopy conductance index for GPP estimation from its capacity. In: Proc. SPIE 10777, Land Surface and Cryosphere Remote Sensing, IV, 107770M. https://doi.org/10.1117/12.2324247.

Muramatsu, K., Ono, K., Soyama, N., Thanyapraneedkul, J., Miyara, A., Mano, M., 2017. Determination of rice paddy parameters in the global gross primary production capacity estimation algorithm using 6 years of JP-MSE flux observation data. J. Agric. Meteorol. 73 (3), 119–132, 7.

Muraoka, H., Noda, H.M., Nagai, S., Motohka, T., Saitoh, T.M., Nasahara, K.N., Saigusa, N., 2013. Spectral vegetation indices as the indicator of canopy photosynthetic productivity in a deciduous broadleaf forest. J. Plant Ecol. 6 (5), 393–407.

Myneni, R.B., Williiams, D.L., 1994. On the relationship between FA-PAR and NDVI. Rem. Sens. Environ. 49, 200–211.

Myneni, R.B., Hoffman, S., Knyazikhin, Y., Privette, J.L., Glassy, J., Tian, Y., Wang, Y., Song, X., Zhang, Y., Smith, G.R., Lotsch, A., Friedl, M., Morisette, J.T., Votava, P., Nemani, R.R., Running, S.W., 2002. Global products of vegetation leaf area and fraction absorbed PAR from year one of MODIS data. Rem. Sens. Environ. 83, 214–231.

Oak Ridge National Laboratory Distributed Active Archive Center (ORNL DAAC), 2008. MODIS collection 5 land product Subsets web service. In: Subset Obtained for MOD09A1 Product Around Sites of NL-Loo, FR-Pue, FR-Hes, IT-Ren, IT-Lav and ES-Agu Site, and Using MODIS Fixed Sites Subsetting Tool. ORNL DAAC, Oak Ridge, Tennessee, USA. http://daac.ornl.gov/cgibin/MODIS/GRcol51/modviz.html. (Accessed 10 June 2016). time period: Jan 1, 2000 to Dec 31, 2015.

Ohta, T., Maximov, T.C., Dolman, A.J., Nakai, T., Molen, M.K., Kononov, A.V., Maximov, A.P., Hiyama, T., Iijima, Y., Moors, E.J., Tanaka, H., Toba, T., Yabuki, H., 2008. Interannual variation of water balance and summer evapotranspiration in an eastern Siberian larch forest over a 7-year period (1998-2006). Agric. For. Meteorol. 148, 1941–1953.

Ono, K., Maruyama, A., Kuwagata, T., Mano, M., Takimoto, T., Hayashi, K., Hasegawa, H., Miyata, A., 2013. Canopy-scale relationships between stomatal conductance and photosynthesis in irrigated rice. Global Change Biol. 19, 2209–2220. https://doi.org/10.1111/gcb.12188.

Owen, K.E., Tenhunen, J., Reichestein, M., Wang, Q., Falge, E., Geyer, R., Xiao, X., Stoy, P., Ammann, C., Arain, A., Aubinet, M., Aurela, M., Bernhofer, C., Chojnicki, B. H., Granier, A., Gruenwald, T., Hadley, J., Heinesch, B., Hollinger, D., Knohl, A., Kutsch, W., Lohila, A., Meyers, T., Moors, E., Moureaux, C., Pilegaard, K., Saigusa, N., Verma, S., Vesala, T., Vogel, C., 2007. Linking flux network measurements to continental scale simulations: ecosystem carbon dioxide exchange capacity under non-water-stressed conditions. Global Change Biol. 13, 734–760. https://doi.org/10.1111/j.1365-2486.2007.01326.x.

Pathre, U., Sinha, A.K., Shirke, P.A., Sane, P.V., 1998. Factors determining the midday depression of photosynthesis in trees under monsoon climate. Trees (Berl.) 12, 472–481.

Peng, Y., Gitelson, A.A., 2012. Remote estimation of gross primary productivity in soybean and maize based on total crop chlorophyll content. Rem. Sens. Environ. 117, 440–448.

Peng, Y., Nguy-Robertson, A., Arkebauer, T., Gitelson, A.A., 2017. Assessment of canopy chlorophyll content retrieval in maize and soybean: implications of hysteresis on the development of generic algorithms. Rem. Sens. 9, 226. https://doi.org/10.3390/rs9030226.

Pessarakli, M. (Ed.), 2005. Handbook of Photosynthesis, second ed. CRC Press, Boca Raton, FL, USA, p. 287.

Polly, H.W., Emmerich, W., Bradford, J.A., Sims, P.L., Johnson, D.A., Saliendra, N.Z., Svejcar, T., Angell, R., Frank, A.B., Phillips, R.L., Snyder, K., Morga, J., 2009. Physiological and environmental regulation of interannual variability in CO_2 exchange on rangelands in the western United States. Global Change Biol. 16, 990–1002. https://doi.org/10.1111/j.1365-2486.2009.01966.x.

Rouse, J.W., Hass, R.H., Schell, J.A., Deerling, D.W., 1973. Monitoring vegetation systems in the great plains with ERTS. In: Third ERTS Symposium, NASA SP-351, I, pp. 309–317.

Running, S., Mu, Q., Zha, M., 2015. MOD17A2H MODIS/terra gross primary productivity 8-day L4 global 500m SIN grid. In: NASA LP DAAC. https://doi.org/10.5067/MODIS/MOD17A2H.006.

Saigusa, N., Yamamotoa, S., Murayamaa, S., Kondo, H., Nishimura, N., 2002. Gross primary production and net ecosystem exchange of a cool temperate deciduous forest estimated by the eddy covariance method. Agric. For. Meteorol. 112, 203–215.

Saito, M., Maksyutov, S., Hirata, R., Richardson, A.D., 2009. An empirical model simulating diurnal and seasonal CO_2 flux for diverse vegetation types and climate conditions. Biogeosciences 6, 585–599.

Sims, D.A., Luo, H., Gamon, J.A., 2002. Relationship between leaf pigment content and spectral reflectance across a wide range of species, leaf structures and development stages. Rem. Sens. Environ. 81, 337–354.

Sims, D.A., Luo, H., Hastings, S., Oechel, W.C., Rahman, A.F., Gamon, J.A., 2006. Parallel adjustments in vegetation greenness and ecosystem CO_2 exchange in response to drought in a Southern California chaparral ecosystem. Rem. Sens. Environ. 103, 289–303.

Soudani, K., Hmimina, G., Dufrene, E., Berveiller, D., Delpierre, N., Ourci-val, J.M., Rambal, S., Joffre, R., 2014. Relationships between photochemical reflectance index and light-use efficiency in deciduous and evergreen broadleaf forests. Rem. Sens. Environ. 144, 73–84.

Steffen, W.L., Walker, B.H., Ingram, J.S., Koch, Q.W., 1992. Global Change and Terrestrial Ecosystems: the Operational Plan. Global Change Report, No.21. The International Geosphere-Biospere Programme: A Study of Global Change (IGBP) of the International Council of Scientific Unions (ICSU), Stockholm, p. 31.

Sulman, B.N., Desai, A.R., Cook, B.D., Saliendra, N., Mackay, D.S., 2009. Contrasting carbon dioxide fluxes between a drying shrub wetland in northern Wisconsin, USA, and nearby forests. Biogeosciences 6 (6), 1115–1126.

Thanyapraneedkul, J., Muramatsu, K., Daigo, M., Furumi, S., Soyama, N., Nishida, K., Nasahara, K.N., Muraoka, H., Noda, H.M., Nagai, S., Maeda, T., Mano, M., Mizoguchi, Y., 2012. A vegetation index to estimate terrestrial gross primary production capacity for the global change observation mission-climate (GCOM-C) second-generation global imager (SGLI) satellite sensor. Rem. Sens. 4 (12), 3689–3720.

Tong, X., Li, J., Yu, Q., Lin, Z., 2014. Biophysical controls on light response of net CO_2 exchange in a winter wheat field in the North China Plain. PLoS One 9 (2), e89469. https://doi.org/10.1371/journal.pone.0089469.

US-Los site's web page: https://ameriflux.lbl.gov/sites/siteinfo/US-Los, DOI: 10.17190/AMF/1246071.

Vermote, E.F., Nazmi, Z.E.S., Christopher, O.J., 2002. Atmospheric correction of MODIS data in the visible to middle infrared: first results. Rem. Sens. Environ. 83, 97–111.

Wullschleger, S.D., 1993. Biochemical limitations to carbon assimilation in C_3 plants – a retrospective analysis of the A/C_i curves from 109 species. J. Exp. Bot. 44 (No. 262), 907–920.

Xiao, X., Hollinger, D., Aber, J., Goltz, M., Davidson, E.A., Zhang, Q., Moore, I.I.I.B., 2004a. Satellite-based modeling of gross primary production in an evergreen needleleaf forest. Rem. Sens. Environ. 89, 519–534.

Xiao, X., Zhang, Q., Braswell, B., Urbanski, S., Boles, S., Wofsy, S., Moore III, B., Ojima, D., 2004b. Modeling gross primary production of temperate deciduous broadleaf forest using satellite image and climate data. Rem. Sens. Environ. 91, 256–270.

Yang, X., Li, R., Jablonski, A., Stovall, A., Kim, J., Yi, K., Ma, Y., Beverly, D., Phillips, R., Novick, K., Xu, X., Lerdau, M., 2023. Leaf angle as a leaf and canopy trait: rejuvenating its role in ecology with new technology. Ecol. Lett. 26, 1005–1020. https://doi.org/10.1111/ele.14215.

You, C., Wang, Y., Tan, X., Zhang, B., Ren, T., Chen, B., Xu, M., Chen, S., 2022. Seasonal and interannual variations of ecosystem photosynthetic characteristics in a semi-arid grassland of northern China. J. Plant Ecol. 15, 961–976. https://doi.org/10.1093/jpe/rtac065.

Zhang, L.M., Yu, G.R., Sun, X.M., Wen, X.F., Ren, C.Y., Fu, Y.L., Li, Q.K., Li, Z.Q., Liu, Y. F., Guan, D.X., Yan, J.H., 2006. Seasonal variations of ecosystem apparent quantum

yield and maximum photosynthesis rate (P_{max}) of different forest ecosystems in China. Agric. For. Meteorol. 137, 176–187.
Zhang, Q., Middleton, E.M., Margolis, H.A., Drolet, G.G., Barr, A.A., Black, T.A., Xiao, X., Braswell, B., Linder, E., Baret, F., Moore III, B., 2009. Can a satellite-derived estimate of the fraction of PAR absorbed by chlorophyll ($FAPAR_{chl}$) improve predictions of light-use efficiency and ecosystem photosynthesis for a broad aspen forest? Rem. Sens. Environ. 113, 880–888.
Zhang, P., Chen, S., Zhang, W., Miao, H., Chen, J., Han, X., Lin, G., 2012. Biophysical regulations of NEE light response in a steppe. J. Plant Ecol. 5 (2), 238–248. https://doi.org/10.1093/jpe/rtr017.